ELSEVIER

Chemical Engineering Science 60 (2005) 6176–6187

Chemical Engineering Science

www.elsevier.com/locate/ces

Influence of the lift force in direct numerical simulation of upward/downward turbulent channel flow laden with surfactant contaminated microbubbles

Andrea Giusti, Francesco Lucci[1], Alfredo Soldati*

Centro Interdipartimentale di Fluidodinamica e Idraulica and Dipartimento di Energetica e Macchine, Università degli Studi di Udine, Via delle Scienze 208, 33100 Udine, Italy

Received 12 November 2004; received in revised form 10 February 2005; accepted 10 February 2005
Available online 28 March 2005

Abstract

In this work, we employ direct numerical simulation of turbulence one-way coupled to Lagrangian tracking to investigate microbubble distribution in upward and downward channel flow. We consider a closed channel flow at $Re_\tau = 150$ and a dispersion of microbubbles characterized by a diameter of 220 μm. Bubbles are assumed contaminated by surfactants (i.e., no-slip condition at bubble surface) and are subject to drag, gravity, pressure gradient forces, Basset history force and aerodynamic lift.

Our results confirm previous findings and show that microbubble dispersion in the wall region is dominated by the action of gravity combined with the lift force. Specifically, in upward flow, bubble rising velocity in the wall region generates a lift force which pushes bubbles to the wall. In downward flow, bubble rising velocity against the fluid generates a lift force which prevents microbubbles from reaching the viscous sublayer.

In the wall region, we observe bubble preferential segregation in high-speed regions in the downflow case, and non-preferential distribution in the upflow case. This phenomenon is related to the effect of the lift force. Compared to experiments, the current lift force model produces larger consequences, this effect being overemphasized in the upflow case in which a large number of bubbles is segregated near the wall. In this case, the resulting bubble wall-peak of concentration outranges experimental results.

These results, so deeply related to the lift force, underline the crucial role of current understanding of the fluid forces acting on bubbles and help to formulate questions about available force models, bubble–bubble interactions and two-way coupling which can be crucial for accurate predictions in the region very near the wall.

Keywords: Bubble; Dispersion; Fluid mechanics; Multiphase flow; Simulation; Turbulence

1. Introduction

The dispersion of microbubbles in turbulent boundary layers has relevance in a number of engineering and environmental applications ranging from bubble columns, gas–liquid reactors, fluidized beds to the transfer mechanisms which couple ocean and atmosphere. In all these applications, the presence of microbubbles, which reportedly are non-uniformly distributed, may significantly change transfer rates. The overall liquid–bubble interface controls gas–liquid transfer, but complex bubble motions also have an influence on overall heat, momentum and mass transfer, playing a crucial role in many industrial and environmental processes. A fashionable application due to current energy awareness is turbulent drag reduction by microbubble injection, recently examined by Madavan et al. (1984), Pal et al. (1988) and Xu et al. (2002) and strictly connected to the change of momentum transfer rate due to microbubbles.

Detailed numerical simulations are an useful tool to improve the current understanding of the local and

* Corresponding author. Tel.: +39 0432558020; fax: +39 0432558027.
E-mail address: soldati@uniud.it (A. Soldati)
URL: http://158.110.32.35 (A. Soldati).
[1] Currently at Department of Mechanical and Aerospace Engineering, University of California, Irvine, CA, USA.

0009-2509/$ - see front matter © 2005 Elsevier Ltd. All rights reserved.
doi:10.1016/j.ces.2005.02.019

instantaneous interactions between bubbles and turbulence and are thus fundamental to predict the overall system evolution. Yet, to the best of our knowledge, there are only few direct numerical simulation (DNS) studies on microbubble behavior in turbulent flows. Among them, Mazzitelli et al. (2003a,b), who studied the behavior of microbubbles in isotropic turbulence, put in evidence the importance of the lift force both for microbubble dispersion and for turbulence modification induced by bubbles. Important results were also obtained for turbulent boundary layers laden with microbubbles (Xu et al., 2002; Ferrante and Elghobashi, 2004). Ferrante and Elghobashi (2004), performed a DNS of a horizontal spatially developing turbulent boundary layer two-way coupled to Lagrangian tracking of pointsize bubbles to investigate on drag reduction by microbubbles. They found that the main effect of microbubbles is to displace away from the wall the quasi-streamwise longitudinal vortical structures which populate the near-wall region (Brooke and Hanratty, 1993; Schoppa and Hussain, 1997), thus reducing the high-shear zones and increasing the low-shear zones.

Bubble behavior in fully developed turbulent boundary layer in duct flow or pipe flow was studied in experimental works. In particular, the works by Serizawa et al. (1975), Hibiki et al. (2004), Kashinsky and Randin (1999) and Beyerlein et al. (1985) led to the conclusion that bubbles injected in a vertical pipe tend to migrate toward the walls in the case of upward flow whereas they tend to concentrate at the core of the pipe in the case of downward flow.

Felton and Loth (2001, 2002) studied experimentally the dispersion of single bubbles in a spatially developing upward turbulent boundary layer. They investigated the specific bubble diameter range of $d_p \in [0.37\text{–}1.2]$ mm, to ensure observing spherical, non-deformable bubbles. They again observed the existence of bubble preferential location which peaks at the wall, this effect being stronger for larger bubbles. A further exploration of this diameter-modulated behavior of microbubble was conducted by Tomiyama et al. (2002) who studied bubble motion in a upward shear flow driven by a moving wall for a wide range of bubble diameters. They observed that, due to shape deformation, larger bubbles (i.e., d_p larger than about 5 mm) move away from the wall, whereas smaller bubbles move towards the wall (in agreement with previous results). They also observed that bubble lateral migration decreased for very small bubbles ($d_p < 0.4$ mm). In connection to the influence of the wall, Takemura and Magnaudet (2003) recently underlined that current lift force model may be inadequate to compute the transverse migration bubble velocity specifically in the wall region: wall effects may be thus crucial in limiting wall-peak accumulation of bubbles.

In previous papers (Marchioli and Soldati, 2002; Marchioli et al., 2003), we characterized the interactions between inertial microparticles and wall turbulence structures, identifying the mechanisms that control the macroscopic non-uniform particle distribution in the wall region of a boundary layer: particle concentration increases in the wall region due to synchronicity between particle transfer and wall turbulence regeneration cycle at the wall. It may be argued that the turbulence structures control bubble transport as well. Yet, due to the very low inertia of the bubbles, we expect preferential bubble concentration to arise from mechanisms which are different from those leading to particle preferential concentration (Maxey, 1987). In the case of microparticles, segregation in boundary layer is due to the large influence of inertia on particle motion in the viscous sublayer, the lift force adding just a quantitative correction to particle behavior. In the case of microbubbles, the aerodynamic lift force is expected to have a dominant effect.

The mechanisms which drive bubbles to the wall in upward flow and away from the wall in downward flow are connected to the driving action of the quasi-streamwise vortices in the wall layer combined to the action of gravity and lift force. Quasi-streamwise vortices have streamwise axis and populate the wall region in the range $z^+ \in [8\text{–}50]$, where they generate jets of outer fluid towards the wall and jets of wall fluid towards the outer region (Schoppa and Hussain, 1997). Both in upward and downward case, bubbles are driven through the last stretch to the wall by the quasi-streamwise vortices. In downward flow, the action of gravity and lift generates a resulting force which pushes bubbles *towards* the inner region of the quasi-streamwise vortices which in turn drive again bubbles away from the wall. In upward flow, gravity and lift combine to push bubbles *away* from the vortex, from which bubbles are thus disengaged. At the same time, they are pushed in a region very near the wall where jet flows directed away from the wall are much less energetic and frequent.

This work focuses precisely on the effect of the lift force on bubble behavior in the wall-region of vertical turbulent channel flow. In particular, we will examine the influence of turbulence on particle distribution in the wall region and we will quantify the role of the forces acting on bubbles and inducing their preferential distribution.

To this object, we ran numerical simulations of upward and downward turbulent channel flow. For each case the trajectories of $O(10^5)$ bubbles were tracked (under one-way coupling assumption) with and without the inclusion of the lift force term in the equation of motion. Our simulations mimic the physics of a dilute swarm of very small microbubbles moving in upward or downward vertical channel flow added with surfactants. Due to the presence of the surfactants, no-slip condition is imposed on bubble surface. Since bubble density is negligible compared to that of the fluid, the bubbles can be considered as *massless spheres* (Ferrante and Elghobashi, 2004), and the effect of bubble internal circulation can be neglected. Due to the small diameters we perform Lagrangian tracking under the pointsize approximation of rigid spherical bubbles.

2. Computational methodology

2.1. Flow field

The flow field was calculated by integrating mass and momentum balance equations made dimensionless using the duct half-width, h, the fluid density, ρ, and the shear velocity, u_τ, defined as

$$u_\tau = \sqrt{\frac{\tau_w}{\rho}}, \tag{1}$$

where τ_w is the shear at the wall. Mass and momentum balance equations in dimensionless form are

$$\frac{\partial u_i}{\partial x_i} = 0 \tag{2}$$

and

$$\frac{\partial u_i}{\partial t} = -u_j \frac{\partial u_i}{\partial x_j} + \frac{1}{Re_\tau} \frac{\partial^2 u_i}{\partial x_j \partial x_j} - \frac{\partial p}{\partial x_i} + \delta_{1,i}, \tag{3}$$

where u_i is the ith component of the velocity vector, $\delta_{1,i}$ is the mean equivalent (i.e., including the effect of gravity) pressure gradient, and $Re_\tau = hu_\tau/\nu$ is the shear Reynolds number. Eqs. (2) and (3) were solved directly using a pseudo-spectral method similar to that used by Kim et al. (1987) to solve the turbulent, closed-channel flow problem and by Lam and Banerjee (1992) to solve the turbulent, open-channel flow problem. The pseudo-spectral method is based on transforming the field variables into wave-number space, using Fourier representations for the periodic streamwise and spanwise directions and a Chebyshev representation for the wall-normal (non-homogeneous) direction. A two level, explicit, Adams–Bashforth scheme for the non-linear terms $u_j \partial u_i/\partial x_j$, and an implicit Crank–Nicolson method for the viscous terms, were employed for time advancement. Details of the method have been published previously (Lam and Banerjee, 1992; Soldati and Banerjee, 1998).

Fig. 1 shows a sketch of the computational domain. The flow between two flat walls is driven by an imposed pressure gradient (determined by the shear Reynolds number) acting in the streamwise direction. Periodic conditions are imposed in streamwise (x) and spanwise (y) directions, whereas no-slip conditions are imposed in wall normal (z) direction.

In the present study, the fluid is water with density (ρ) of 1000 kg m^{-3} and kinematic viscosity (ν) of 10^{-6} m^2 s^{-1}. Since the equivalent pressure gradient is the same for all simulations, the shear velocity is 7.5×10^{-3} m s^{-1}, and the shear Reynolds number, Re_τ, is equal to 150. The mean velocity is 0.1125 m s^{-1} and the Reynolds number based on mean velocity and half-duct width is ≈ 2250. All variables are normalized by the wall shear velocity u_τ, the fluid density ρ and the fluid kinematic viscosity ν. All dimensionless (wall units) variables are characterized by the superscript $+$. The computational domain is $1885 \times 942 \times 300$ wall units in x, y and z with $64 \times 64 \times 65$ nodes. The spacing of collocation points in the streamwise and spanwise directions is $\Delta x^+ \approx 30$, $\Delta y^+ \approx 15$ in wall units. The first collocation point away from the wall is at $z^+ = 0.18$; this grid resolution is sufficient to describe the significant length scales in the channel flow. The time step used was $\Delta t^+ = 3.6 \times 10^{-2}$ in wall time units.

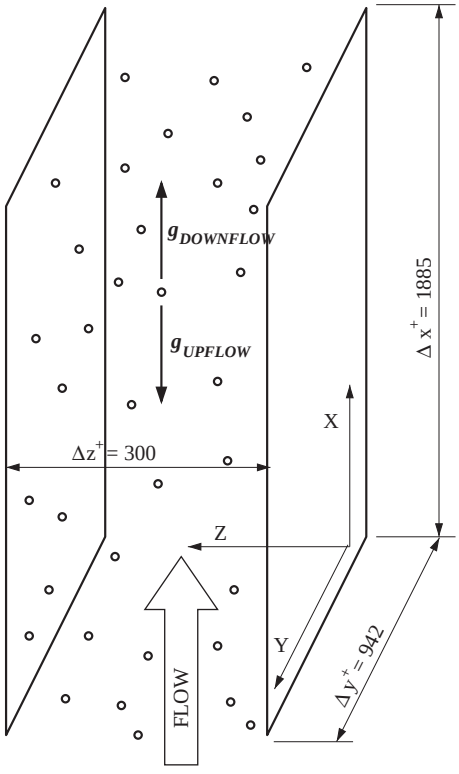

Fig. 1. Sketch of the computational domain.

Even though the grid is slightly less refined compared to other DNS databases (Kim et al., 1987), the large-scale wall structures are well resolved. In Fig. 2, we compare the 64^3 results against results obtained with a 128^3 grid (twice the resolution in each direction). From a statistical viewpoint, the results obtained with the two different grids match closely, both collapsing on the results obtained by Lyons et al. (1991) for the same Reynolds number. We examined in detail the evolution of the wall structures below $z^+ = 80$. We found hardly any difference in the shape, extent and duration of the structures which dominate wall transfer mechanisms—large-scale quasi-streamwise vortices, low-speed streaks, sweeps and ejections.

2.2. Bubble dynamics

A Lagrangian method is used to compute the trajectory of microbubbles. Equations used to calculate time-evolution

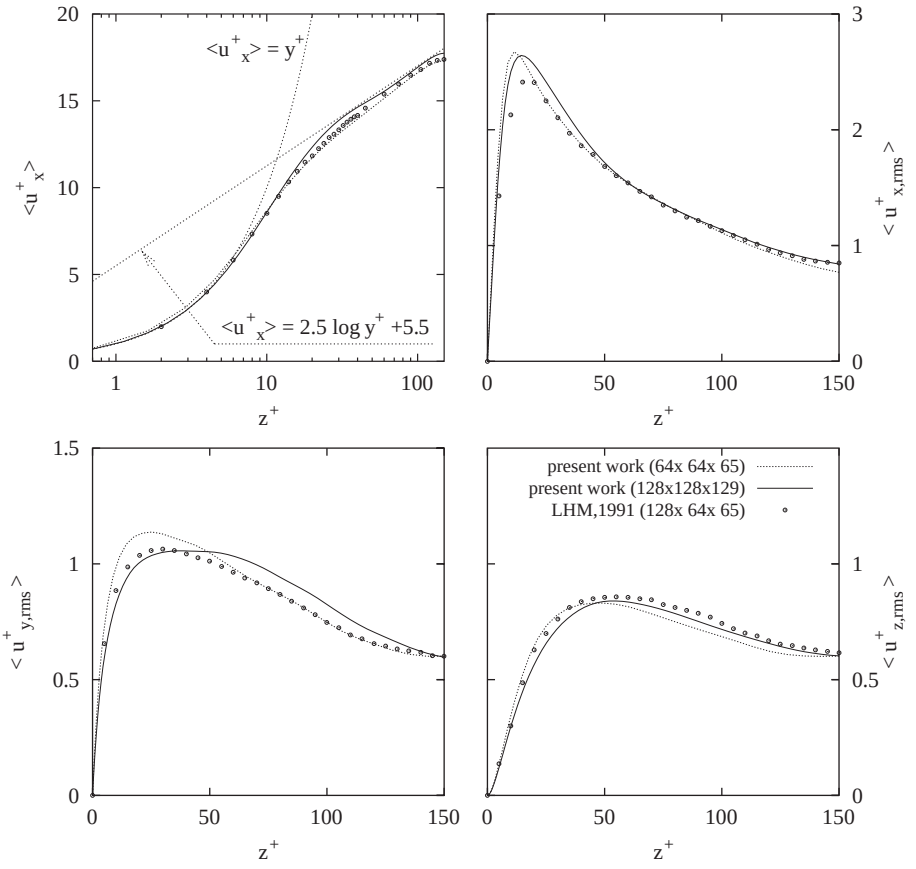

Fig. 2. Comparison between Eulerian fluid statistics (mean velocity and root mean squares) obtained from the present simulations (grid $64 \times 64 \times 65$), simulations with more refined grid (grid $128 \times 128 \times 129$), and data from Lyons et al. (1991) (grid $128 \times 64 \times 65$).

of bubble position and velocity are

$$\frac{\mathrm{d}\mathbf{x}_p}{\mathrm{d}t} = \mathbf{v}_p, \tag{4}$$

$$\begin{aligned}\frac{\mathrm{d}\mathbf{v}_p}{\mathrm{d}t} = &\left(1 - \frac{\rho}{\rho_p}\right)\mathbf{g} + \frac{(\mathbf{u} - \mathbf{v}_p)}{\tau_p}\left(1 + 0.15Re_p^{0.687}\right)C_W \\ &+ \frac{\rho}{\rho_p}\frac{\mathrm{D}\mathbf{u}}{\mathrm{D}t} + C_L\frac{\rho}{\rho_p}[(\mathbf{u} - \mathbf{v}_p)\boldsymbol{\omega}] \\ &+ \frac{9\mu}{d_p\rho_p\sqrt{\pi\nu}}\int_0^t\left(\frac{\mathrm{d}\mathbf{u}}{\mathrm{d}t} - \frac{\mathrm{d}\mathbf{v}_p}{\mathrm{d}t}\right)\frac{\mathrm{d}\tau}{(t-\tau)^{0.5}} \\ &+ \frac{\rho}{2\rho_p}\left(\frac{\mathrm{D}\mathbf{u}}{\mathrm{D}t} - \frac{\mathrm{d}\mathbf{v}_p}{\mathrm{d}t}\right),\end{aligned} \tag{5}$$

where $\mathbf{x}_p$ and $\mathbf{v}_p$ are the bubble instantaneous position and velocity, $\mathbf{u}$ and $\boldsymbol{\omega}$ are fluid velocity and vorticity (calculated at bubble position), d_p and ρ_p are bubble diameter and density and $\mathbf{g}$ is gravitational acceleration.

Right-hand side terms in Eq. (5) represent the forces per unit of mass acting on a bubble and describe the effect of gravity, drag, pressure gradient, aerodynamic lift, time-history Basset and added mass force, respectively. This equation is similar to the equation of motion for small rigid spheres discussed by Maxey and Riley (1983), in which we neglected the second-order terms (related to ∇u_i) due to the small size of the bubbles (Hinze, 1987; Rizk and Elghobashi, 1985). We also included the non-linear correction coefficient (Schiller and Naumann, 1933) to modify the Stokesian drag force for larger bubble Reynolds number defined as $Re_p = |\mathbf{u} - \mathbf{v}_p|d_p/\nu$.

In our simulations we consider bubbles to behave as small rigid spheres. The hypothesis of spherical shape holds if bubble diameter is small enough to satisfy the condition $Eo < 0.2$, where $Eo = d_p^2|\rho_p - \rho|g/\sigma_s$ is the Eotvos (or Bond) number (Michaelides, 2003) and σ_s is the surface tension at fluid/bubble interface. This hypothesis is verified for air bubbles with diameter smaller than about 1 mm which move in water. If water contains surfactants, no-slip condition can be applied at bubble interface (Ferrante and Elghobashi, 2004). Furthermore bubble internal circulation effects are neglected due to the low ratio of bubble density to fluid density. These assumptions justify the coefficients in Eq. (5).

In the drag force term, τ_p is the characteristic time of the bubble, defined as $\tau_p = (d_p^2\rho_p)/(18\nu\rho)$. When bubbles approach the walls, drag modification due to the wall is modelled using the correction coefficient C_W as in Fukagata et al. (1999). Equations used to calculate C_W, in directions

parallel ($_\parallel$) and orthogonal ($_\perp$) to the wall, are

$$C_{W_\parallel} = \left[1 - \frac{9}{16}\left(\frac{d}{2z}\right) + \frac{1}{8}\left(\frac{d}{2z}\right)^3 - \frac{45}{256}\left(\frac{d}{2z}\right)^4 - \frac{1}{16}\left(\frac{d}{2z}\right)^5\right]^{-1},$$

$$C_{W_\perp} = \left[\left\{1 - \frac{9}{8}\left(\frac{d}{2z}\right) + \frac{1}{2}\left(\frac{d}{2z}\right)^2\right\}\left\{1 - \exp\left(-2.686\left(\frac{2z}{d} - 0.999\right)\right)\right\}\right]^{-1}, \quad (6)$$

where the term $d/2z$ indicates the ratio between bubble radius and the distance between wall and bubble center.

In the lift force term, the coefficient C_L is a function of bubble Reynolds number and of the dimensionless parameter Sr_p defined as $Sr_p = |(\mathbf{u}-\mathbf{v}_p)\boldsymbol{\omega}|d_p/|\mathbf{u}-\mathbf{v}_p|^2$. We calculated C_L as (see McLaughlin, 1991; Kurose and Komori, 1999):

$$C_L = \begin{cases} C_{L_{\mathrm{McL}}} = \left[5.816\left(\dfrac{Sr_p}{2Re_p}\right)^{0.5} - 0.875\dfrac{Sr_p}{2}\right]\dfrac{3}{4Sr_p}\dfrac{J(\varepsilon)}{2.255} & \text{for } Re_p < 1, \\ C_{L_{\mathrm{McL}}}\dfrac{5 - Re_p}{4} + C_{L_{\mathrm{KK}}}\dfrac{Re_p - 1}{4} & \text{for } 1 < Re_p < 5, \\ C_{L_{KK}} = \left[K_0\left(\dfrac{Sr_p}{2}\right)^{0.9} + K_1\left(\dfrac{Sr_p}{2}\right)^{1.1}\right]\dfrac{3}{4Sr_p} & \text{for } Re_p > 5, \end{cases} \quad (7)$$

where we indicate with $C_{L_{\mathrm{McL}}}$ the coefficient calculated using the formula by McLaughlin (1991). The function $J(\varepsilon)$ is reported in McLaughlin (1991), the variable ε being defined as $\varepsilon = (Sr_p/Re_p)^{0.5}$. $J(\varepsilon)$ is a correction factor added by McLaughlin (1991) to the expression of the lift force model reported by Saffman (1965) to extend its validity to situations where the hypothesis of negligible Re_p is not ensured. The coefficient $C_{L_{\mathrm{KK}}}$ is calculated as in Kurose and Komori (1999), K_0 and K_1 being tabulated values depending on Re_p. The coefficient C_L, used to calculate the lift force acting on bubbles, is set equal to $C_{L_{\mathrm{McL}}}$ for low particle Reynolds numbers($Re_p < 1$) and equal to $C_{L_{\mathrm{KK}}}$ for high particle Reynolds numbers ($Re_p > 5$). A linear interpolation between the coefficients $C_{L_{\mathrm{McL}}}$ and $C_{L_{\mathrm{KK}}}$ is used to calculate C_L for intermediate values of particle Reynolds number ($1 < Re_p < 5$).

The Basset history force has been considered in Eq. (5), since previous studies showed that it may be an important term in the momentum balance of a bubble; e.g., in the experiments of Takemura and Magnaudet (2004), the Basset force is observed to reach values almost equal to half the value of the buoyancy force.

An accurate calculation of the forces acting on the particle requires accurate evaluation of the instantaneous fluid velocity at the particle location. Since a pseudo-spectral method is used to solve the flow field equations (Eqs. (2) and (3)), a pseudo-spectral interpolation gives the highest accuracy level, but requires high computational work. Kontomaris et al. (1992), employed Lagrange polynomials in the homogeneous directions and Chebyshev polynomials in the non-homogeneous direction. This procedure showed to be highly accurate and the computational work requirement was smaller by roughly the factor $(6/N_x)(6/N_y)$ than the computational work requirement for a fully spectral evaluation of the fluid velocity field at the centre of the particle, which involves summing the Fourier–Chebyshev series (Soldati et al., 1997). In recent papers, several authors who investigated the behavior of large swarms of particles used time-efficient lower-order interpolation schemes, proving they were accurate enough to maintain statistical accuracy (van Haarlem et al., 1998) and to preserve local resolution for the small scales of the boundary layer (Rouson and Eaton, 2001). In the present work, however we used a sixth-order Lagrange interpolation which has high accuracy and relatively low computational cost.

To keep the average volume fraction of bubbles in the computational domain constant in time, when a bubble exits one of the domain boundaries in streamwise or spanwise direction it is reinjected accordingly to the periodic conditions of the fluid field. Bubble–wall interaction is computed by enforcing rigid elastic rebound.

3. Numerical simulations

Single phase simulations (i.e., with no bubbles) were run until the flow reached a statistically steady state. Then 10^5 microbubbles, with density $\rho_p = 1.3\,\mathrm{kg/m^{-3}}$ and diameter $d_p = 220\times10^{-6}\,\mathrm{m}$ (values in wall units are $\rho_p^+ = 1.3\times10^{-3}$ and $d_p^+ = 1.65$), were injected in the flow field. The initial position of the bubbles was randomly chosen within the computational domain and the initial velocity of each bubble was set equal to that of the fluid at bubble position. The overall volume and mass fractions of the dispersed bubbles are equal respectively to $\Phi_V = 4.42\times10^{-4}$ and $\Phi_M = 5.74\times10^{-7}$. Bubble characteristic time, corrected to account for added mass effect, is $\tilde{\tau}_p = \tau_p[1 + \rho/(2\rho_p)] = 1.348\times10^{-3}\,\mathrm{s}$. The corresponding value in wall units is $\tilde{\tau}_p^+ = 7.58\times10^{-2}$. Assuming a value for the surface tension at the water/air interface equal to $\sigma_s = 7.28\times10^{-2}\,\mathrm{N\,m^{-1}}$, the Eotvos number of the bubbles is $Eo = 6.25\times10^{-3}$: the condition $Eo < 0.2$ is satisfied and bubbles can be considered spherical. We calculated a posteriori bubble Reynolds number and we found

it ranging from a value slightly lower than 2 in the centre of the channel to about 1 when the wall is approached.

Upflow and downflow cases were simulated by imposing $\mathbf{g} = -g\hat{\mathbf{e}}_x$ and $\mathbf{g} = g\hat{\mathbf{e}}_x$ in Eq. (5), respectively (see Fig. 1). For each case a simulation with and without the action of the lift force was run. The total simulation period is $\Delta T = 19.2$ s (in wall units $\Delta T^+ = 1080$), sufficient for a fluid particle with a speed equal to the average fluid velocity to move through the entire streamwise length of the channel more than eight times. Time-step advancement, for calculation of both the fluid velocity field and the microbubble motion, was set equal to $\Delta t = 6.4 \times 10^{-4}$ s (in wall units $\Delta t^+ = 3.6 \times 10^{-2}$), nearly half of the corrected bubble characteristic time $\tilde{\tau}_p$ and, accordingly to the Nyquist theorem, sufficient to provide a faithful reproduction of bubble transient behavior (Elghobashi and Truesdell, 1992).

4. Results

4.1. Distribution statistics

In Fig. 3, the time-evolution of microbubble number concentration profiles is shown as a function of the distance z^+ from the channel wall in the upward flow case. Data shown in Fig. 3(a) are relative to the simulation without lift. Data shown in Fig. 3(b) are relative to the simulation with lift. Profiles are normalized to the initial channel uniform bubble number concentration, c_0. A logarithmic scale is used for the z^+-axis to expand the near-wall region. If the lift force is not considered, there is very little time change of the bubble number concentration as shown in Fig. 3(a). We can observe only a slight increase "at the wall". In general, however, bubbles appear to behave like passive tracers without showing macroscopic non-uniformities in the wall-normal direction. The importance of the lift force emerges clearly if we observe Fig. 3(b). There is a continuous bubble accumulation at the wall in the region $z^+ < 2$, and a corresponding depletion in the buffer layer. Even if profiles do not appear to have reached a steady state, we stopped the simulation because the one-way coupling approach that we adopted is no more reliable to describe the behavior of the swarm of bubbles in proximity of the walls when such high values of concentration are reached (two-way coupling and bubble–bubble collision models should be included).

In Fig. 4, the time-evolution of microbubble number concentration profiles is shown as a function of the distance z^+ from the channel wall in the downward flow case. Data shown in Fig. 4(a) were computed with all forces in Eq. (5) acting on the bubbles with the exception of the lift force. Data shown in Fig. 4(b) were computed including also the lift force. In the absence of lift force, bubble number density profiles appear similar to those for the upper flow, showing a slight increase only in the region very near to the wall ($z^+ < 2$). Again, a sharp deviation from this behavior is obtained if we include the action of the lift force as shown in

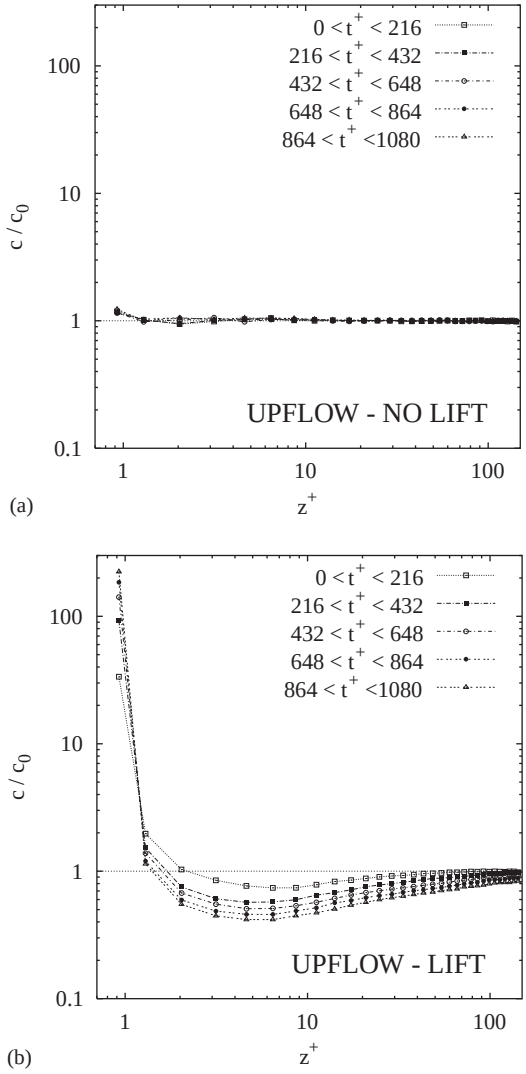

Fig. 3. Time evolution of microbubbles concentration profile in the upflow case: (a) simulation without lift and (b) simulation with lift.

Fig. 4(b). As soon as the simulation starts, all bubbles are promptly pushed away from the wall region and there is virtually no bubble present in the region $z^+ < 10$. Particles appear rather uniformly distributed in the rest of the channel and profiles seem to reach a steady state rather soon.

Our results obtained from simulations with the lift force are in qualitative agreement with previous experimental studies on spherical bubbles behavior in turbulent flows near vertical walls. Both bubble migration towards the wall in upflow case and away from the wall in downflow case were observed in experiments (Serizawa et al., 1975; Hibiki et al., 2004; Kashinsky and Randin, 1999; Ogasawara et al., 2004). However, from a quantitative point of view, our simulations seem to overpredict bubble lateral migration with respect to experimental data (Felton and Loth, 2001; Tomiyama et al., 2002; Ogasawara et al., 2004), especially for the upflow case when the high values of bubble concentration at the wall obtained from our simulation ($c/c_0 \simeq 200$) are not

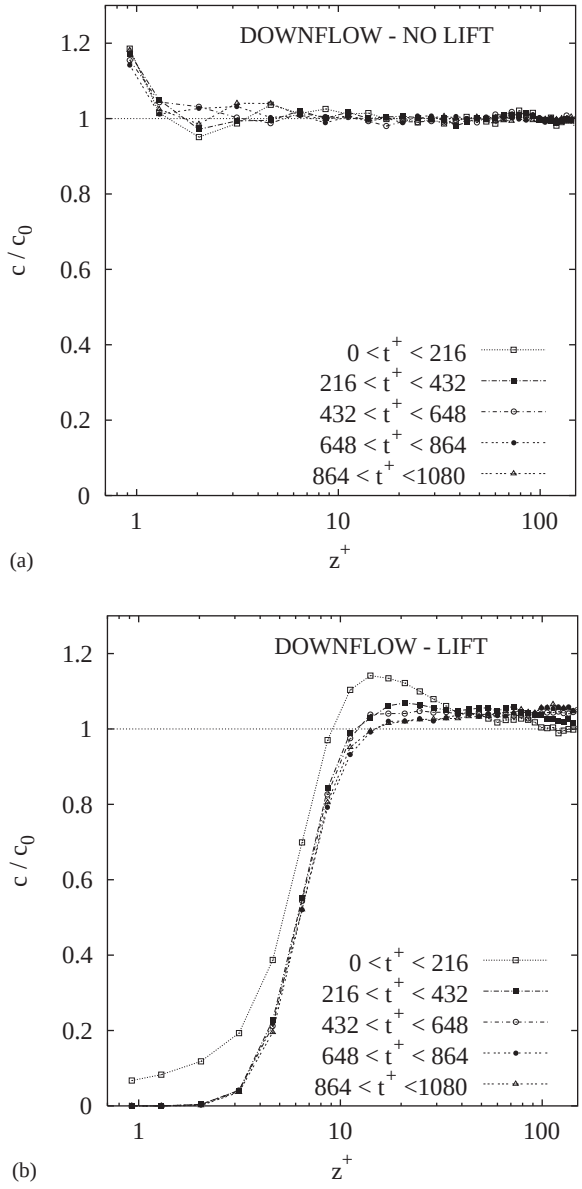

Fig. 4. Time evolution of microbubbles concentration profile in the downflow case: (a) simulation without lift and (b) simulation with lift.

observed in the experiments. For instance, Ogasawara et al. (2004) considered an upward flow with conditions similar to those of our simulation, except for bubble diameter which is about 1 mm, and observed wall-peak void fraction values ranging from about 9 to about 16 times the average void fraction occupied by the bubbles (see Fig. 5 in Ogasawara et al., 2004; cases with surfactants).

A similar discrepancy between the concentration profiles obtained from experiments and from our simulations is not observed in the downflow case, in which bubbles are swept away from the wall and reach a stationary condition. This suggests that our model overpredicts the lateral migration of bubbles near the walls, where high bubble concentration are observed in the upflow case. One possible cause of this overestimation is the fact that our one-way coupled simulation does not consider the concentration effect (i.e., bubble–bubble interaction), that in real experiments limits the phenomenon of bubble accumulation at the wall and allows the bubbles to reach a steady concentration profile. A second possible explanation is that our model overestimates the lift force, as it will be discussed in a following section concerning the forces acting on bubbles.

In a previous paper, Colin and Legendre (2001) computed the trajectories of bubble swarms in a large eddy simulation of upward, downward and microgravity turbulent channel flow and compared numerical results with experimental observations. Even though they considered clean bubbles, their results are in qualitative agreement with ours. Specifically, they show that the combined effect of gravity and lift is responsible for bubble migrating towards the wall in upflow case and away from the wall in downflow case. In microgravity case, no significant bubble transverse migration is observed.

4.2. Velocity statistics

Mean velocity statistics were obtained by averaging over a time window of $\Delta t^+ = 200$ (sufficient for a fluid particle moving at the average fluid velocity to cover a distance greater than one channel streamwise length). We noticed that statistics were not changing by increasing the time window up to 600.

In Fig. 5 we show bubble wall normal velocity for both upflow and downflow cases. Fig. 5(a) refers to the simulation without lift whereas Fig. 5(b) refers to the simulation with lift. From Fig. 5(a) we observe that if there is no lift force the average wall normal velocity is uniformly zero, corresponding to the absence of wall accumulation observed in Figs. 3(a) and 4(a), with the exception of a very slight increase in the region adjacent to the wall. If we observe Fig. 5(b), we may appreciate first the large negative (i.e., wallward) wall normal drift velocity for the upflow case. In the downward flow case we may observe that wall normal bubble velocity is uniformly around zero. However, we may observe that, since there is no bubble in the region immediately adjacent to the wall, the velocity profile is interrupted at $z^+ \simeq 2$ (as indicated by the black arrow).

In Fig. 6 we show the time-averaged streamwise mean velocity of microbubbles. In Fig. 6(a) we show upward and downward flow cases calculated without lift. The dashed line represents the time-averaged streamwise mean velocity for the fluid. In the upward flow case bubbles move faster than the fluid in the upward direction (empty squares) with an almost uniform lead due to the net buoyancy. In the downward flow case bubbles move slower than the fluid in the downward direction (solid circles) with a lag which is uniform almost everywhere. Both for upward and downward flow, in the region immediately adjacent to the wall ($z^+ < 2$) bubble velocity becomes closer to fluid velocity due to the

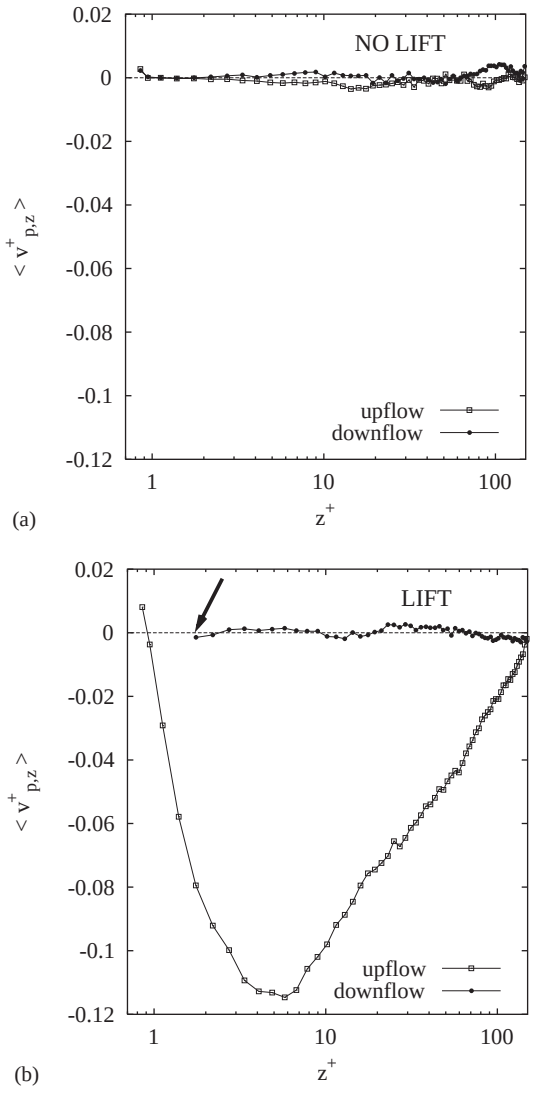

Fig. 5. Microbubbles wall-normal averaged velocity: (a) simulation without lift and (b) simulation with lift.

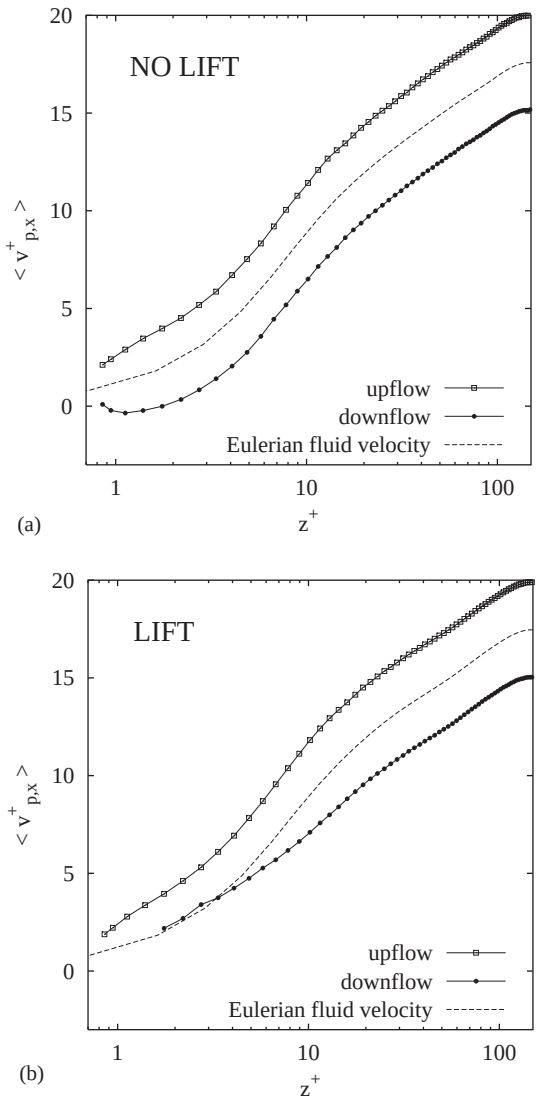

Fig. 6. Microbubbles streamwise averaged velocity: (a) simulation without lift and (b) simulation with lift.

wall correction which increases the drag force in the wall proximity.

In Fig. 6(b) we show upward and downward flow cases calculated with the full Eq. (5) including the lift force. In the upflow case, the time-averaged streamwise mean bubble velocity is similar to that calculated in the no-lift case. However, if we observe the behavior of the mean streamwise velocity for the downflow case we notice that bubbles almost match the fluid velocity at $z^+ \simeq 10$. This indicates that below $z^+ = 10$ bubbles move downward at the same velocity as the fluid. Of course this behavior may not be explained with the influence of the wall and needs a detailed analysis (see description of Fig. 7). We want to remark here that for $z^+ < 4$ (see Fig. 4(b), few bubbles are present in the wall region to average.

In Fig. 7 we show the time-averaged streamwise mean velocity profile of the fluid *measured at bubble position*. Our object is to verify whether the turbulence field sampled by bubbles corresponds to the average turbulence field. In Fig. 7(a) we show data computed for the no-lift case. Fluid velocity profiles computed at bubble position collapse onto each other and onto the Eulerian flow field demonstrating no preferential distribution, and thus no preferential flow field sampling, by the bubbles. In Fig. 7(b) we show data computed for the lift force case. In the upflow case, we observe that bubbles tend to sample fluid regions with streamwise velocity slightly larger than the mean for $z^+ > 6$ and fluid regions with streamwise velocity slightly lower than the mean for $z^+ < 6$. In the downward flow case, we observe that bubbles sample fluid regions with velocity largely higher than the mean for $z^+ < 10$. In particular, bubbles sample fluid regions with streamwise velocity exceeding the fluid mean streamwise velocity of a fraction of the bubble rising velocity shown in Fig. 6(a), thus bubbles flow downward almost

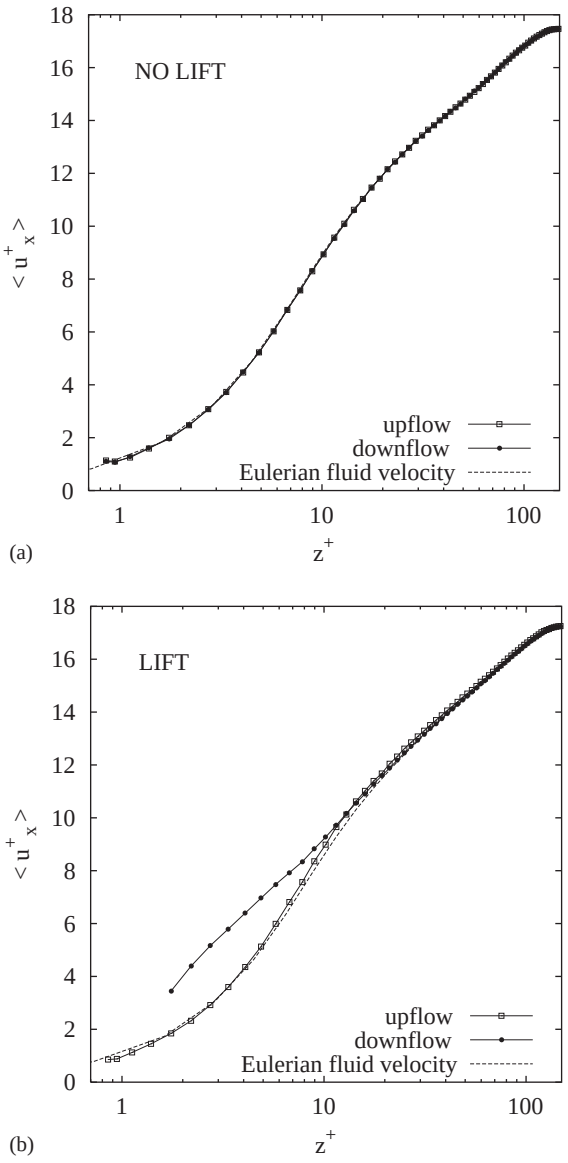

Fig. 7. Fluid streamwise velocity averaged on bubble positions: (a) simulation without lift and (b) simulation with lift.

with the fluid in the region for $z^+ < 10$. This preferential sampling seems due to the combined action of buoyancy and lift forces and the effect of the quasi-streamwise vortices that populate the turbulent near wall region. Specific investigation of these mechanisms is still an object of our investigations.

4.3. Forces acting on bubbles

In Figs. 8 and 9 we show streamwise and wall normal components of the forces acting on bubbles in upward and downward flow cases. Spanwise components are rather irrelevant for macroscopic behavior in the present configuration. Figs. 8 and 9 refer, respectively, to simulations without and with the action of the lift force on bubbles. In both figures, the upper graphics (a and b) show the statistics of the streamwise component of the forces, whereas the lower (c and d) show the statistics of the wall normal component. The graphics on the left (a and c) refers to upflow simulations whereas that on the right (b and d) refers to downflow cases.

Results for the force streamwise component show that bubble buoyancy is the largest force and it is counterbalanced by the drag force only. The intensity of buoyancy force does not depend on whether the lift force is considered or not. The sign of the buoyancy force is positive in upflow cases (Figs. 8a and 9a) and negative in downflow cases (Figs. 8b and 9b).

If we consider the wall normal component, no dominant effect is observed in simulations without lift, both in the upflow (Fig. 8c) and in the downflow (Fig. 8d) case. When lift force is considered, it becomes the dominant effect (counterbalanced by the drag force only) when the wall is approached ($z^+ < 40$). This can be observed both in the upflow (Fig. 9c) and in the downflow (Fig. 9d) case. Lift force is negative (i.e., directed toward the wall) in the upflow and positive (i.e., directed away from the wall) in the downflow case.

For simulated conditions, the Basset force effect is negligible with respect to the dominant effects of buoyancy (in streamwise direction) and of lift (in wall-normal direction) and it does not modify qualitatively bubble behavior.

As previously observed, a quantitative comparison with experimental data of microbubbles in upward vertical flow (Ogasawara et al., 2004) shows that we overestimate bubble migration towards the wall and that one possible cause is that the employed numerical model overestimates the lift force in the near wall region. This is probably due to the fact that in our simulation the model of the lift force does not consider any wall-effect, which would induce a transverse lift force pushing particles away from the wall (Magnaudet et al., 2003). Since microbubbles ($d_p = 0.22$ mm) are considered in the present work, a further possible cause of the overestimation of the lift effect may be related to bubble size, as suggested by the experiments of Tomiyama et al. (2002) on bubble behavior in upward simple shear flows: in these experiments the measured "net transverse lift coefficient" is almost constant and towards the wall for bubble diameter ranging from 0.5 to 4 mm but tends to smaller values for small bubble diameters (lower than 0.5 mm). This decrease of the lift effect acting on bubbles with such small diameters is not considered in the model employed to calculate the lift coefficient in our simulation.

It is important to remark here that we believe that the lack of the wall-effect in the lift model is the main cause of the overestimation of the lift force, since large differences between simulated and experimentally observed bubble behaviors results only in the upflow case, where most of the bubbles move in the wall region ($z^+ < 10$). In the downflow case, bubbles do not reach the wall region where the lift force may be influenced by the wall.

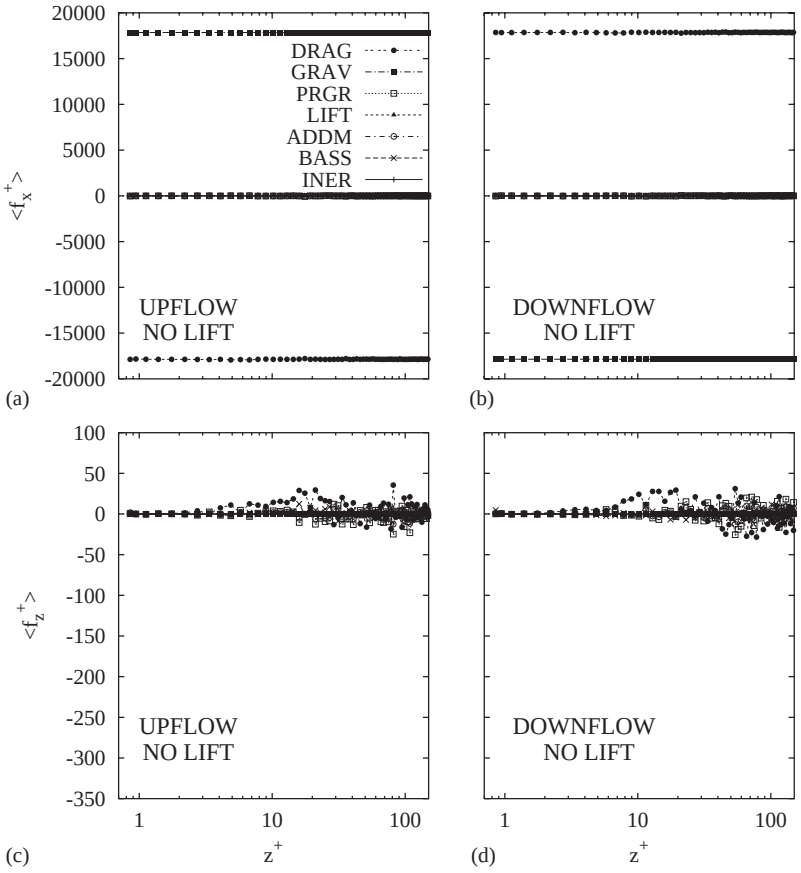

Fig. 8. Streamwise and wall-normal components of the forces acting on bubbles in simulations without lift: (a) upflow, streamwise direction; (b) downflow, streamwise direction; (c) upflow, wall-normal direction; and (d) downflow, wall-normal direction.

5. Conclusions and future developments

The accurate prediction of microbubble distribution in turbulent boundary layer is crucial to quantify transfer rates in a number of individual and environmental applications ranging from bubble columns to ocean–atmosphere coupling phenomena.

In this work, we used direct numerical simulation (DNS) of turbulence in channel flow at $Re_\tau = 150$ to study the behavior of microbubbles ($d_p = 220\,\mu m$) in upward and downward flow. We considered large swarms ($O[10^5]$) of pointsize, spherical and surfactant contaminated bubbles one-way coupled to the fluid and we computed their time-dependent space distribution solving the momentum equation for each single bubble in a Lagrangian reference frame. The momentum equation included the influence of drag, inertia and added mass, gravity, pressure gradient, Basset and lift force. We considered the wall effect by correcting the drag force model according to Fukagata et al. (1999). We run benchmark calculations not including the lift force and we obtained an almost uniform bubble distribution in the entire channel both in upward and downward flow. In both cases, bubbles sample uniformly the flow field and they show just the expected buoyancy-induced velocity difference compared to the fluid in the streamwise direction.

When the lift force is added, bubble behavior changes dramatically and simulations reproduce the qualitative behavior observed in experiments. In the upflow case, a net bubble migration is produced toward the wall and quickly most of the bubbles are trapped in the viscous sublayer ($z^+ < 5$). In the downflow case, a net bubble migration is produced away from the wall and virtually no bubble is observed in the wall region ($z^+ < 10$).

In our simulations we did not consider any wall correction to the lift force. The presence of the wall (Takemura and Magnaudet, 2003) may reduce the intensity of the lift force in upward flow, thus reducing our apparently overestimated (Felton and Loth, 2001, 2002) bubble preferential wall segregation.

If the lift force is present, bubbles no longer sample uniformly the turbulent flow field. In particular, we observed that in downward flow bubbles are selectively present in flow regions where the instantaneous streamwise velocity is larger than the mean. This produces an average streamwise velocity for the bubbles which is almost that of the fluid thus compensating the effect of the buoyancy.

These results are connected to the strongly non-homogeneous flow structure of the boundary layer where quasi-streamwise vortices drive bubbles towards the wall and reentrain them away from the wall. In upward flow, a bubble

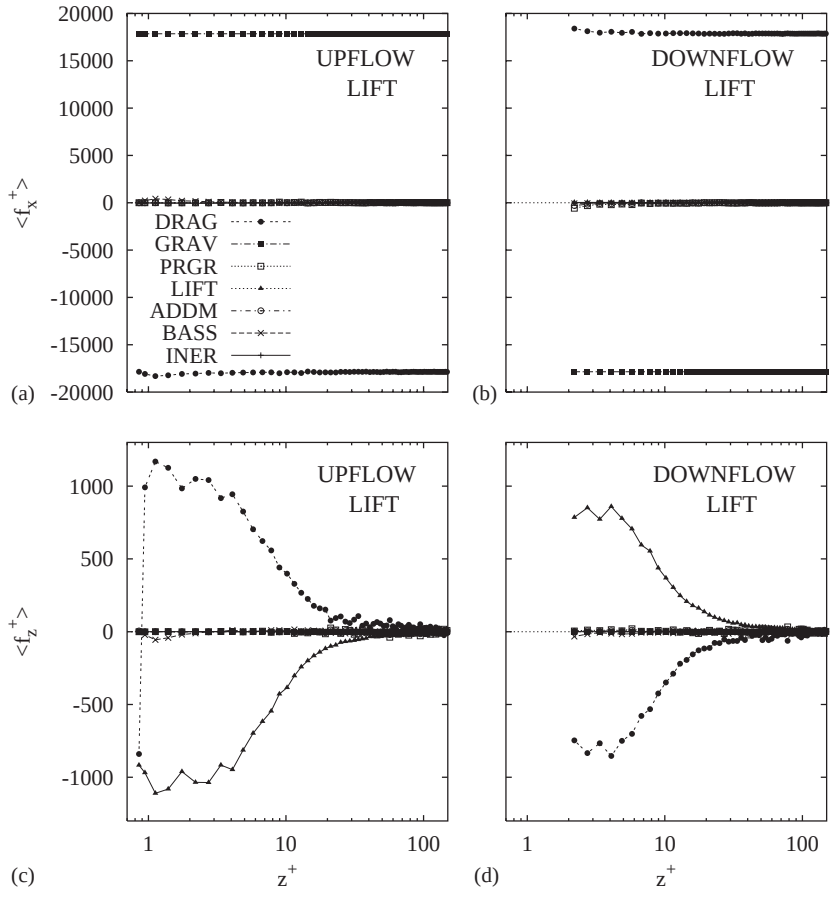

Fig. 9. Streamwise and wall-normal components of the forces acting on bubbles in simulations with lift: (a) upflow, streamwise direction; (b) downflow, streamwise direction; (c) upflow, wall-normal direction; and (d) downflow, wall-normal direction.

driven to the wall by a quasi-streamwise vortex undergoes the combined action of gravity and lift and is pushed away from the vortex in the viscous sublayer, where flow ejections away from the wall are less frequent and less energetic. In downward flow, the action of gravity and lift is reversed, the bubble is pushed towards the vortex core and is quickly reentrained in the outer flow. Bubbles are thus prevented from reaching the wall region and are kept in flow regions where the streamwise velocity is larger than the mean (Marchioli and Soldati, 2002).

Further research is required to investigate deeper in the phenomena occurring in the wall region. In particular, more detailed models of the lift force should be tested into our simulations including a dependence of the lift coefficient on other parameters such as bubble Eotvos number (Tomiyama, 2004), bubble diameter (Tomiyama et al., 2002), wall presence (Magnaudet et al., 2003; Takemura and Magnaudet, 2003).

Also, a detailed investigation of bubble trajectory in connection with the dynamics of the wall structures should be pursued including the use of two-way coupling methods to clarify the modifications of transfer coefficients (Ferrante and Elghobashi, 2004).

A final remark is related to the simulation of upflow cases with the lift force. Even though *wall corrected* lift models can limit the large concentration peak at the wall, bubble–bubble and bubble–wall interaction models will be crucial to capture the relevant physics of the phenomena.

Acknowledgements

Financial support from Italian Ministry for University and Research in the frame of PRIN program under Grant no. 2003099224_002 is gratefully acknowledged. A.G. is grateful to Marina Campolo, Cristian Marchioli and Fabio Sbrizzai for their help.

References

Beyerlein, S.W., Cossmann, R.K., Richter, H.J., 1985. Prediction of bubble concentration profiles in vertical turbulent two-phase flow. International Journal of Multiphase Flow 11 (5), 629–641.

Brooke, J.W., Hanratty, T.J., 1993. Origin of turbulence-producing eddies in channel flow. Physics of Fluids A 5, 1011–1022.

Colin, C., Legendre, D., 2001. Bubble distribution in turbulent shear flows: experiments and numerical simulations on single bubbles. Proceedings of the Fourth International Conference on Multiphase Flows, New Orleans, USA.

Elghobashi, S., Truesdell, G.C., 1992. Direct simulation of particle dispersion in a decaying isotropic turbulence. Journal of Fluid Mechanics 242, 655–700.

Felton, K., Loth, E., 2001. Spherical bubble motion in a turbulent boundary layer. Physics of Fluids 13 (9), 2564–2577.

Felton, K., Loth, E., 2002. Diffusion of spherical bubbles in a turbulent boundary layer. International Journal of Multiphase Flow 28, 69–92.

Ferrante, A., Elghobashi, S., 2004. On the physical mechanisms of drag reduction in a spatially-developing turbulent boundary layer laden with microbubbles. Journal of Fluid Mechanics 503, 345–355.

Fukagata, K., Zahrai, S., Bark, F.H., Kondo, S., 1999. Influences of the near-wall drag correction in a lagrangian simulation of particulate turbulent channel flow. In: Banerjee, S., Eaton, J.K. (Eds.), Proceedings of the First International Symposium on Turbulence and Shear Flow Phenomena. Begell House Inc., New York, pp. 259–264, ISBM 1-56700-135-1.

van Haarlem, B., Boersma, B.J., Nieuwstadt, F.T.M., 1998. Direct numerical simulation of particle deposition onto a free-slip and no-slip surface. Physics of Fluids 10, 2608–2620.

Hibiki, T., Goda, H., Kim, S., Ishii, M., Uhle, J., 2004. Structure of vertical downward bubbly flow. International Journal of Heat and Mass Transfer 47, 1847–1862.

Hinze, J.O., 1987. Turbulence. In: Clark, B.J. (Ed.), McGraw-Hill Classic Textbook Reissue. McGraw-Hill, New York, pp. 628–629.

Kashinsky, O.N., Randin, V.V., 1999. Downward bubbly gas–liquid flow in a vertical pipe. International Journal of Multiphase Flow 25, 109–138.

Kim, J., Moin, P., Moser, R., 1987. Turbulence statistics in fully developed channel flow at low Reynolds number. Journal of Fluid Mechanics 177, 133–166.

Kontomaris, K., Hanratty, T.J., Mc Laughlin, J.B., 1992. An algorithm for tracking fluid particles in a spectral simulation of turbulent channel flow. Journal of Computational Physics 103, 231–242.

Kurose, R., Komori, S., 1999. Drag and lift forces on a rotating sphere in a linear shear flow. Journal of Fluid Mechanics 384, 183–206.

Lam, K., Banerjee, S., 1992. On the condition of streak formation in bounded flows. Physics of Fluids A 4, 306–320.

Lyons, S.L., Hanratty, T.J., McLaughlin, J.B., 1991. Large-scale computer simulation of fully developed turbulent channel flow with heat transfer. International Journal of Numerical Methods in Fluids 13, 999–1028.

Madavan, N., Deutsch, S., Merkle, C., 1984. Reduction of turbulent skin friction by microbubbles. Physics of Fluids 27, 356–363.

Magnaudet, J., Takagi, S., Legendre, D., 2003. Drag, deformation and lateral migration of a buoyant drop moving near a wall. Journal of Fluid Mechanics 476, 115–157.

Marchioli, C., Soldati, A., 2002. Mechanisms for particle transfer and segregation in a turbulent boundary layer. Journal of Fluid Mechanics 468, 283–315.

Marchioli, C., Giusti, A., Salvetti, M.V., Soldati, A., 2003. Direct numerical simulation of particle wall transfer and deposition in upward turbulent pipe flow. International Journal of Multiphase Flow 29, 1017–1038.

Maxey, M.R., 1987. The motion of small spherical particles in a cellular flow field. Physics of Fluids 30, 1915–1928.

Maxey, M.R., Riley, J.J., 1983. Equation of motion for a small rigid sphere in a nonuniform flow. Physics of Fluids 26 (4), 883–889.

Mazzitelli, I.M., Lohse, D., Toschi, F., 2003a. On the relevance of the lift force in bubbly turbulence. Journal of Fluid Mechanics 488, 283–313.

Mazzitelli, I.M., Lohse, D., Toschi, F., 2003b. The effect of microbubbles on developed turbulence. Physics of Fluids 15 (1), L5–L8.

McLaughlin, J.B., 1991. Inertial migration of a small sphere in linear shear flows. Journal of Fluid Mechanics 224, 261–274.

Michaelides, E.E., 2003. Hydrodynamic force and heat/mass transfer from particles, bubbles, and drops—The Freeman Schoolar Lecture. Journal of Fluids Engineering 125, 209–238.

Ogasawara, T., Tagawa, Y., Fujiwara, A., Takagi, S., Matsumoto, Y., 2004. Proceedings of the Third International Symposium on Two-Phase Flow Mod. and Exp., Pisa 22–24 September 2004. In: Celatta, G.P., Di Marco, P., Mariani, A., Shah, R.K. (Eds.), Two-Phase Flow Modelling and Experimentation, Vol. 1, pp. I–135. Edizioni ETS, Pisa.

Pal, S., Merkle, C., Deutsch, S., 1988. Bubble characteristics and trajectories in a microbubble boundary layer. Physics of Fluids 31 (4), 744–751.

Rizk, M.A., Elghobashi, S.E., 1985. The motion of a spherical particle suspended in a turbulent flow near a plane wall. Physics of Fluids 28 (3), 806–817.

Rouson, D.W., Eaton, J.K., 2001. On the preferential concentration of solid particles in turbulent channel flow. Journal of Fluid Mechanics 428, 149–169.

Saffman, P.G., 1965. The lift on a small sphere in a slow shear flow. Journal of Fluid Mechanics 22, 385–400 (and Corrigendum, 1968, Journal of Fluid Mechanics 31, 624).

Schiller, V.L., Naumann, A., 1933. Über die grundlegenden Berechnungen bei der Schwerkraftaufbereitung. Zeitschrift des Vereines Deutscher Ingenieure 77 (12), 318–320.

Schoppa, W., Hussain, F., 1997. Genesis and dynamics of coherent structures in near-wall turbulence. In: Panton, R. (Ed.), Self-sustaining Mechanisms of Wall Turbulence. Advances in Fluid Mechanics, vol. 15. Computational Mechanics Publications, pp. 385–422.

Serizawa, A., Kataoka, I., Michiyoshi, I., 1975. Turbulence structure of air–water bubbly flow-II. Local properties. International Journal of Multiphase Flow 2, 235–246.

Soldati, A., Banerjee, S., 1998. Turbulence modification by large scale organized electrohydrodynamic flows. Physics of Fluids 10, 1742–1756.

Soldati, A., Casal, M., Andreussi, P., Banerjee, S., 1997. Lagrangian simulation of turbulent particle dispersion in electrostatic precipitators. A.I.Ch.E. Journal 43, 1403–1413.

Takemura, F., Magnaudet, J., 2003. The transverse force on clean and contaminated bubbles near a vertical wall at moderate Reynolds number. Journal of Fluid Mechanics 495, 235–253.

Takemura, F., Magnaudet, J., 2004. The history force on a rapidly shrinking bubble rising at finite Reynolds number. Physics of Fluids 16 (9), 3247–3255.

Tomiyama, A., 2004. Proceedings of the Third International Symposium on Two-Phase Flow Mod. and Exp., Pisa, 22–24 September 2004. In: Celatta, G.P., Di Marco, P., Mariani, A., Shah, R.K. (Eds.), Two-Phase Modelling and Experimentation, Vol. 1, pp. I–3. Edizioni ETS, Pisa.

Tomiyama, A., Tamai, H., Zun, I., Hosokawa, S., 2002. Transverse migration of single bubbles in simple shear flows. Chemical Engineering Science 57, 1849–1858.

Xu, J., Maxey, M.R., Karniadakis, G.E., 2002. Numerical simulation of turbulent drag reduction using micro-bubbles. Journal of Fluid Mechanics 468, 271–281.